

Reconstructing the Nasal Septum from Instrument Motion During Septoplasty Surgery

Matthew S. Holden^{a,b,*}, Molly O'Brien^a, Anand Malpani^a, Hajira Naz^a, Ya-Wei Tseng^a, Lisa Ishii^c, S. Swaroop Vedula^a, Masaru Ishii^c, Gregory Hager^a

^aMalone Center for Engineering in Healthcare, Johns Hopkins University, Baltimore, USA

^bSchool of Computer Science, Carleton University, Ottawa, Canada

^cDepartment of Otolaryngology - Head and Neck Surgery, Johns Hopkins University School of Medicine, Baltimore, USA

Abstract.

Purpose: Surgery involves modifying anatomy to achieve a goal. Reconstructing anatomy can facilitate surgical care through surgical planning, real-time decision support, or anticipating outcomes. Tool motion is a rich source of data that can be used to quantify anatomy. This work develops and validates a method for reconstructing the nasal septum from unstructured motion of the Cottle elevator during the elevation phase of septoplasty surgery, without need to explicitly delineate the surface of the septum.

Approach: The proposed method uses iterative closest point registration to initially register a template septum to the tool motion. Subsequently, statistical shape modelling with iterative most likely oriented point registration is used to fit the reconstructed septum to Cottle tip position and orientation during flap elevation. Regularization of the shape model and transformation is incorporated. The proposed methods were validated on ten septoplasty surgeries performed on cadavers by operators of varying experience level. Pre-operative CT images of the cadaver septums were segmented as ground-truth.

Results: We estimated reconstruction error as the difference between the projections of the Cottle tip onto the surface of the reconstructed septum and the ground-truth septum segmented from the CT image. We found translational differences of $2.74(2.06 - 2.81)mm$ and a rotational differences of $8.95(7.11 - 10.55)^\circ$ between the reconstructed septum and the ground-truth septum (median (inter-quartile range)), given the optimal regularization parameters.

Conclusions: Accurate reconstruction of the nasal septum can be achieved from tool tracking data during septoplasty surgery on cadavers. This enables understanding of the septal anatomy without need for traditional medical imaging. This result may be used to facilitate surgical planning, intra-operative care, or skills assessment.

Keywords: surgical navigation, statistical shape modelling, surgical data science, surgical skills assessment, nasal septoplasty.

*Matthew S. Holden, matthew.holden@carleton.ca

1 Introduction

Surgery involves manipulating patient anatomy to achieve a clinical goal. In fact, many surgical procedures are indicated by pathological alterations of geometry of anatomical structures. For example, deformities in the nasal septum lead to difficulty breathing. Surgery to treat deformities involves correcting the geometry of the anatomical structures. It follows that the extent of deformity affects difficulty or complexity of the surgical intervention and influences its outcomes.

1 Clearly, quantifying geometry of anatomical structures can have a significant impact on surgical
2 care, for example, by facilitating surgical planning, supporting intraoperative decision-making, and
3 predicting outcomes.¹

4 Reconstructing anatomy is necessary to quantify change in geometry due to surgery. Most
5 research on reconstructing anatomy has relied upon videos of the surgical field; however, little
6 research exists on reconstructing anatomy using instrument motion data. For the large part, during
7 surgery, instruments constantly interact with anatomical surfaces, and thus, the point cloud formed
8 by the instrument tip positions is a rich source of data to reconstruct anatomy. In fact, instru-
9 ment motion is known to be an effective data source to assess surgical skill.²⁻⁴ Existing methods
10 primarily reconstruct anatomy from a highly structured point clouds obtained in well controlled
11 experimental settings. To our knowledge, there is no method developed to reconstruct geometry
12 using unstructured point clouds obtained from routine surgical care in the operating room.

13 *1.1 Anatomical Surface Reconstruction*

14 Several previous works have attempted to reconstruct anatomical surfaces from point cloud data
15 systematically sampled on the surface of the anatomy. These methods can be distinguished based
16 on whether they use a priori statistical knowledge about the shape of the surface.⁵ Hoppe et al.⁶
17 proposed one of the first and most common methods on surface reconstruction without a prior. One
18 of the earliest and most common methods for surface reconstruction with a prior is using statistical
19 shape models by Cootes et al.⁷ A review of surface reconstruction techniques from structured or
20 unstructured point clouds is provided by Lim and Haron.⁸

1 *1.2 Nasal Septoplasty Surgery*

2 Nasal septoplasty is a common head and neck surgery to correct a structural deviation in the nasal
3 septum in patients presenting with difficulty in breathing.⁹ The shape of the septum alters geometry
4 of the nasal airway, resulting airflow, and consequently causes patient symptoms. From a surgical
5 perspective, septum shape affects technical complexity of the surgery, choice of surgical approach,
6 and the likelihood that surgery improves patient outcomes.

7 Despite being critical for surgical care and outcomes, surgeons largely operate without ade-
8 quate information on shape of the septum for routine septoplasty procedures. Although patients
9 may undergo anterior rhinoscopy or nasal endoscopy in the clinic before surgery,¹⁰ these investi-
10 gations do not allow full reconstruction of the nasal septum. While CT imaging allows reconstruc-
11 tion of the nasal septum, it is not routinely indicated unless there is concomitant pathology such
12 as chronic rhinosinusitis requiring surgery.^{11,12} Furthermore, intraoperative endoscopy can allow
13 video reconstruction of the septum shape but endoscopic surgery is also not routinely indicated or
14 reimbursed for septoplasty. Finally, even when CT imaging or endoscopic video is available, they
15 do not allow assessment of intraoperative evolution of the surgical procedure.

16 We suggest that the shape of the septum and its deviation can be understood by intra-operatively
17 analyzing motion data from tracked instruments used in septoplasty surgery. More specifically,
18 this work considers Cottle motion during the flap elevation phase of septoplasty. The flap elevation
19 phase in septoplasty is a critical phase involving the separation of the mucosal flap from the nasal
20 septum using the Cottle elevator. Our clinical experience indicates this is one of the most difficult
21 phases of septoplasty. Details on flap elevation are provided by Fettman et al.¹³



Fig 1 Photograph of a Cottle elevator used for flap elevation during septoplasty surgery. Both tips can be used for elevation.

1 *1.3 Objective*

2 This work develops and validates a method for reconstructing the nasal septum from the motion
3 of the surgical instrument tip during the elevation phase of septoplasty surgery. The proposed
4 methods do not require the septum's surface to be explicitly delineated, but rather, use tool motion
5 data passively acquired during surgery. The proposed methods to automatically recover geometry
6 of anatomy in the surgical field, which informs disease severity, technical complexity, and extent
7 of surgery as well as their association with postoperative outcomes.

8 **2 Methods**

9 *2.1 Experimental Setup*

10 We follow the same data collection protocol as Ahmidi et al.² Instruments were tracked during
11 the surgery using an NDI Aurora electromagnetic tracking system (Northern Digital Inc.) with
12 6DOF pose sensors (root-mean-square position accuracy $0.70mm$ and orientation accuracy 0.30°).
13 A sensor was affixed to the patient's forehead as a reference; sensors were affixed to all applicable
14 surgical instruments, including the Cottle elevator (Figure 1) used during elevation of the mucosal
15 flap. Sensors were affixed using specially designed instrument mounts to minimize the effects of
16 electromagnetic field distortions due to the ferromagnetic instruments.²

17 Pivot calibration was performed separately for each tool, to determine the tool's tip. Prior to
18 each septoplasty, the operator used the Cottle to draw a circle around the patient's nose and a line

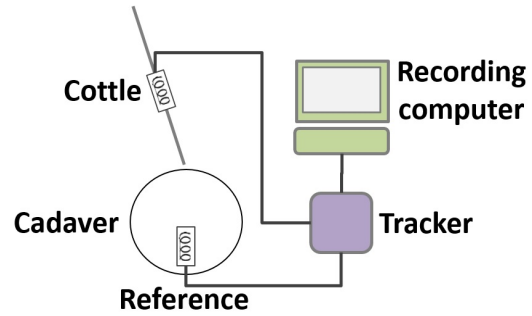


Fig 2 Photograph of ongoing tracked septoplasty surgery (left) and diagram of data collection setup (right).

1 along the dorsum of the nose.

2 During surgery, the ongoing phase and instrument in use is manually annotated by a trained
3 observer. These annotations are revised post-operatively by the same observer to ensure quality.
4 In particular, the beginning and end of the nose circle, nose line, and flap elevation phase are
5 delineated.

6 2.2 *Fitting the Shape Model to Trajectory Data*

7 The following steps provides a high-level overview of the proposed method for reconstructing the
8 nasal septum (Figure 3). Details of the method are presented in the subsequent sections.

- 9 1. Computation of the statistical shape model of the septum.
- 10 2. Initial alignment of the mean septum via ICP registration.
- 11 3. Computation of the orientation of points on the instrument's trajectory.
- 12 4. Combined registration and shape modelling of the septum using IMLOP registration with
13 regularization.

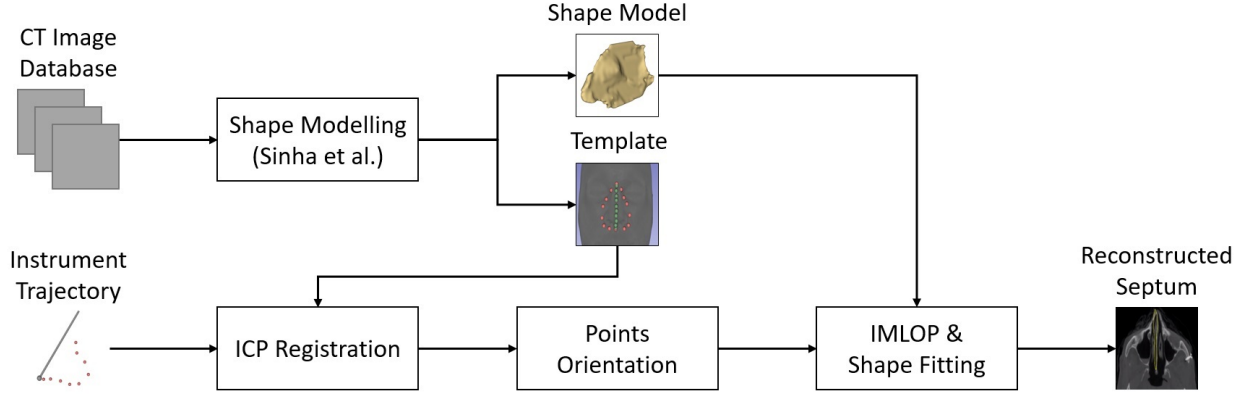


Fig 3 Block diagram illustration of the proposed method for reconstructing the nasal septum.

1 2.2.1 Statistical Shape Model of the Septum

2 We built a statistical shape model of the nasal septum following the work of Sinha et al.¹⁴ We used
 3 a pre-existing database of 50 CT images of the head. First, we generated a template CT image
 4 of the head by iteratively registering all of the images to a target image, and computing the mean
 5 displacement field. The method is based on the ANTs software;¹⁵ it uses a non-linear deforma-
 6 tion with cross-correlation as the similarity metric. Subsequently, we segmented the septum of
 7 the template CT image and computed the segmented septums in all CT images by applying the
 8 displacement field to it. Finally, we generated a statistical shape model for the septum from the 50
 9 segmented septums.

10 The number of modes of variation in our shape model of the septum, M , is a parameter that
 11 may be adjusted. A total of 7140 points r_i were sampled on the shape. We define \bar{r} to be the mean
 12 shape, $E = [e_1, \dots, e_M]$ to be eigenvectors of the shape model, and $\lambda_1, \dots, \lambda_M$ to be the eigenvalues
 13 of the shape model.

1 2.2.2 Initial Registration of the Septum

2 As an initial step, we roughly register the template CT image to the reference sensor on the patient's
3 forehead in the following way (Equation 1). First, in the template CT image, we manually select
4 fiducial points evenly distributed around the nose on a circle NC^{Temp} and along the dorsum of
5 the nose NL^{Temp} with sufficient density to capture local features (see Figure 4). Subsequently,
6 we register these fiducials to the Cottle tip trajectory during the drawing of the nose circle NC^{Ref}
7 and nose line NL^{Ref} on the dorsum using a multi-part iterative closest point (ICP) method. In our
8 multi-part ICP, we only permit correspondences between points on the nose circles and between
9 points two nose lines on the dorsum (i.e. points on the nose circle are not permitted to correspond
10 to points on the nose line). We perform this multi-part ICP over 312 initial rotations¹⁶ and select
11 the registration with the smallest fiducial registration error. This provides an initial estimate of the
12 pose of the nasal septum aligned with the Cottle tip motion during elevation in the reference sensor
13 coordinate frame.

$$T_{init}^{Ref \rightarrow Temp} = ICP((NC^{Ref}, NL^{Ref}), (NC^{Temp}, NL^{Temp})) \quad (1)$$

14 2.2.3 Computing Trajectory Points Orientation

15 We fit the shape model to the trajectory data from the Cottle tip during the elevation phase, where
16 the start and stop times of the phase is manually annotated by the trained observer. Consider the
17 sequence of tool trajectory points $p_i^{Ref}, i = 1, \dots, T$, as manually annotated by the trained observer.
18 We computed orientation for trajectory points on the surface of the septum in the following way:

- 19 1. Determine which points are associated with the surface of the septum.

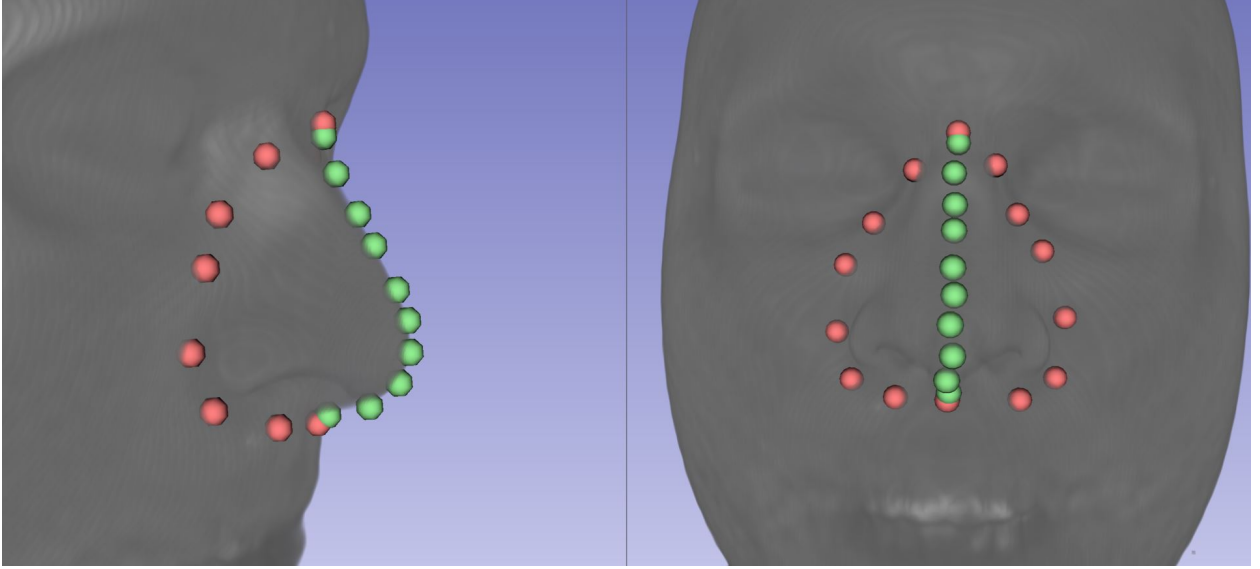


Fig 4 Sagittal (left) and coronal (right) views of fiducial points selected on nose circle (red) and nose line (green) on the dorsum in the template CT image.

- 1 2. Approximate the orientation for each trajectory point p_i^{Ref} to associate it with one side of the
- 2 septum.

3 First, we discard outlying points during elevation (e.g. points where the Cottle is outside the

4 nasal cavity) via a nearest neighbour approach (Equation 2). Those points p_i^{Ref} whose mean dis-

5 tance MND_i to the nearest neighbours $N(p_i^{Ref})$ was more than one standard deviation σ_{MND}

6 greater than the mean of the mean distances \overline{MND} to neighbours was removed. We used 12 near-

7 est neighbours. This eliminates the sparse extraction motions observed outside the nasal cavity.

$$MND_i = \frac{1}{|N(p_i^{Ref})|} \sum_{q \in N(p_i^{Ref})} |p_i^{Ref} - q|$$

$$MND_i \begin{cases} < \overline{MND} + \sigma_{MND} \Rightarrow \text{keep} \\ > \overline{MND} + \sigma_{MND} \Rightarrow \text{discard} \end{cases} \quad (2)$$

1 Second, to estimate the local septum normal at each point on the trajectory, we observe that
 2 the Cottle is rotated 180 degrees about its axis when operating on the other side of the nose. We
 3 compute the direction vector the spoon tip is facing for each point s_i , and the signed orthogonal
 4 distance from each point d_i to the initial estimate of the septal plane \hat{n}, x_0 (see section 2.2.2). We
 5 use a Gaussian mixture model on the combined orientation and distance to determine two clusters
 6 of poses. The mixture model is initialized based on the signs of the distances. We assume these
 7 clusters c_i represent motion on the two sides of the septal plane. We assign these points to have
 8 orientation v_i^{Ref} normal to the initially estimated septum (Equation 3).

$$\begin{aligned}
 c_i &= GMM([s_i, d_i]) \\
 v_i^{Ref} &= \begin{cases} \hat{n}, & \text{if } c_i = 0 \\ -\hat{n}, & \text{if } c_i = 1 \end{cases} \quad (3)
 \end{aligned}$$

9 Additionally, we randomly resample the points on the trajectory p_i with replacement to get
 10 an equal number of points on each side of the initial estimate of the septal plane. For each side,
 11 the number of points after resampling was equal to the number of points on the side of the initial
 12 septum originally with fewer points.

13 2.2.4 Combined Registration and Shape Modelling

14 Once we have the oriented points within the nasal cavity from the trajectory, we seek to fit the
 15 septum shape model to these oriented points. To this end, we iteratively update the transforma-
 16 tion $T_i^{Ref \rightarrow Temp}$ via the Iterative Most Likely Oriented Point (IMLOP) registration protocol¹⁷ and

1 update the shape model parameters, in the following way (details provided subsequently).

- 2 1. Register the oriented septum surface with the oriented trajectory points via Iterative Most
- 3 Likely Orientated Points registration.
- 4 2. Fit the shape model to the trajectory points via active shape modelling.
- 5 3. Iterate.

6 We register the oriented septum surface r_i^{Temp}, u_i^{Temp} , where the orientation is taken as the

7 surface normals, with the oriented trajectory points p_i^{Ref}, v_i^{Ref} , where orientation is computed as

8 described above. We use the standard IMLOP registration (Equation 4)¹⁷ with inlier ratio λ_i .

$$T^{Ref \rightarrow Temp} = IMLOP \left(\{ [p_i^{Ref}, v_i^{Ref}] \}, \{ [r_i^{Temp}, u_i^{Temp}] \}; \lambda_i \right) \quad (4)$$

9 We fit the septum shape model to the trajectory points using standard active shape modelling

10 methods.^{7,18} Correspondences between shape model points and trajectory points are determined

11 from IMLOP registration. We clip the shape model weights to be within three standard deviations

12 (Equation 5).¹⁹

$$b = E^T \left(T^{Ref \rightarrow Temp} p_i^{Ref} - \bar{r}^{Temp} \right)$$

$$\text{Clip: } -3\sqrt{\lambda_j} \leq b_j \leq 3\sqrt{\lambda_j} \quad (5)$$

$$r_i^{Temp} = \bar{r}^{Temp} + Eb$$

13 These two steps are performed iteratively until a stopping criteria is reached. We iterated until

14 the change in the root mean square error (which is a weighted sum of position and orientation error)

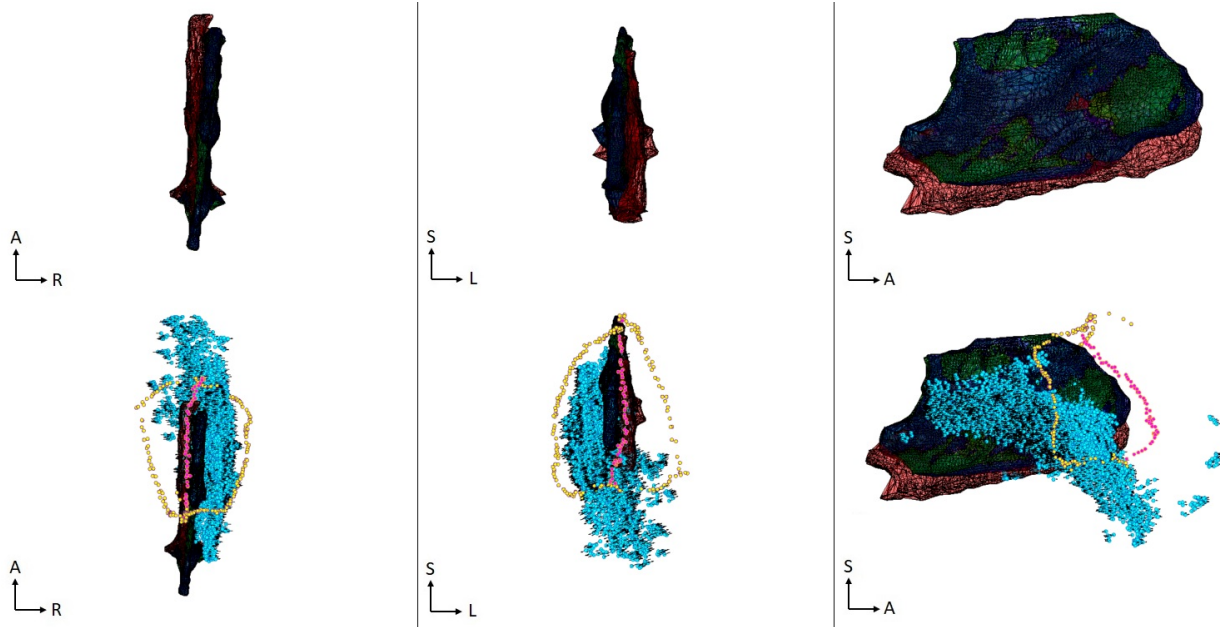


Fig 5 Initial (blue) and full (green) reconstructions of the septum from Cottle tip trajectory, with the ground-truth septum (red) for the axial (left), sagittal (centre), and coronal (right) views. Points along the trajectory with their estimated orientation are illustrated (cyan and black). Nose circle (yellow) and nose line (magenta) illustrated.

1 between corresponding points during the IMLOP phase dropped below a pre-defined threshold of
 2 0.01^{17} (Figure 5).

3 2.2.5 Regularization of the Fitting

4 We hypothesize that our initial rough estimation of the septum could be an accurate fit. Thus,
 5 we introduce two methods for regularization in our methods: (1) regularization of the IMLOP
 6 registration and (2) regularization of the shape model parameters.

7 To regularize the registration, we sample a small subset of oriented points on the septum sur-
 8 face. We add these points to the set of oriented trajectory points. Thus, the IMLOP registration is
 9 biased towards the initial registration. We control regularization by tuning the proportion, λ_t of the
 10 sample used.

11 To regularize the shape model parameters, we use the standard L2 regularization (i.e. ridge
 12 regularization). This regularization is applied just prior to clipping. It biases the shape model

1 towards the mean septum shape in the absence of otherwise compelling evidence. The shape
2 model regularization is taken to be proportional to the dataset size and is controlled by tuning the
3 regularization parameter λ_r .

$$b_j = \frac{b_j}{1 + \lambda_r \frac{|r_i|}{|p_i|}} \quad (6)$$

4 2.3 Validation Study on Cadaver Septums

5 We validated the accuracy of the proposed methods for septum reconstruction on a set of twelve
6 cadaver septums. Participants performed septoplasty surgeries on cadaver heads using standard
7 procedures over the course of 10 months at Johns Hopkins Hospital. Seven of the septoplasties
8 were performed by two expert surgeons; five of the septoplasties were performed by medical or
9 engineering personnel.

10 Prior to each septoplasty surgery, four to seven fiducial screws were affixed to the skull. Fidu-
11 cials were placed at the temporal, frontal, and maxillary regions of the skull on both the left and
12 right sides. Subsequently, a CT image of the cadaver head was acquired and a trained human man-
13 ually segmented the nasal septum from the CT image. Prior to each septoplasty surgery, a tracked
14 pointer tool was pivoted on each screw head to allow for rigid fiducial registration between the CT
15 images and the reference tracker attached to the skull. By registering the segmented septum into
16 the reference tracker coordinate frame, we get a ground-truth estimate of the nasal septum.

17 2.3.1 Measures of Reconstruction Accuracy

18 First, we compute the topological accuracy of the reconstruction. We project the Cottle tip at each
19 timestamp onto the closest point on both the reconstructed septum and ground-truth septum. We

1 filter out motions off the septum’s surface by a distance threshold. We report the distance between
2 these projections (Projection Position Differences), as well as the angle between the smoothed
3 local normals at these projections (Projection Orientation Differences). Large differences in angles
4 (greater than 90 degrees) due to errors in translation are filtered out. Subsequently, we consider the
5 overall accuracy of the pose of the reconstructed septum.

6 Next, we measure the overall error in pose of the reconstructed septum. We compute the
7 distance between the centroids of the reconstructed and ground-truth septums (Translational Dis-
8 tance), and we compute the angles between the principal components of the ground-truth and
9 reconstructed septums (Rotational Distance). We also report these measures broken down into
10 their in-plane and out-of-plane components (computed using the normal vector to the planar ap-
11 proximation of the ground-truth septum).

12 Finally, we report two standard measures of similarity: the median Hausdorff Distance and the
13 Dice Similarity Coefficient.

14 2.3.2 *Hyperparameter Search*

15 We performed a grid search over the space of hyperparameters using a leave-one-septum-out ap-
16 proach. That is, we reconstructed each septum using the set of hyperparameters achieving the best
17 performance on all other septums. The adjusted hyperparameters were the number of modes of
18 variation in the shape model M , the inlier ratio in IMLOP λ_i , the registration regularization λ_t ,
19 and the shape model regularization λ_r (Equation 7). The search space for these hyperparameters
20 were determined manually by empirical testing on the dataset.

$$\begin{aligned}
M &= \{10, 20, 50\} \\
\lambda_i &= \{0.6, 1.0\} \\
\lambda_t &= \{10^{-2}, 10^{-1.5}, 10^{-1}\} \\
\lambda_r &= \{10^1, 10^2, 10^3\}
\end{aligned}
\tag{7}$$

1 As a comparison, we report the same measures for septums estimated as an infinite plane using
2 the method proposed by Ahmidi et al.² and septums reconstructed using just the initial registration
3 phase (see section 2.2.2).

4 2.3.3 *Confounding Factors*

5 We investigated the effect of two confounding factors on the reconstructions: septal deflection and
6 operator skill level. Septal deflection was determined from the manual segmentations of the sep-
7 tums from CT images. It was computed as the 95th percentile distance between a planar estimate
8 of the septum and the medial point of the segmentation. Operator skill level was determined by
9 appointment status.

10 To determine the effect of the confounding factors, we compute the rank correlation (with p-
11 value) of the measures of reconstruction accuracy against the septal deflection and operator skill
12 level.

13 **3 Results**

14 Septal reconstruction succeeded in all cases with complete datasets (Figure 6). Due to technical
15 difficulties with the tool tracking equipment, however, complete datasets for septoplasty surgery

Table 1 Accuracy metrics for septum reconstruction. Results from the planar fit (planar),² initial registration (initial), and for the full reconstruction (full). Values are reported as median (inter-quartile range). The best performing method for each metric is indicated in bold.

Metric	Planar ²	Initial	Full
Projected Position Differences (<i>mm</i>)	2.85(2.56 – 3.45)	2.80(2.30 – 3.11)	2.74(2.06 – 2.81)
Projected Orientation Differences (°)	11.86(6.64 – 16.13)	9.35(7.35 – 11.54)	8.95(7.11 – 10.55)
Translational Distance (<i>mm</i>)	-	7.56(5.15 – 15.22)	11.22(6.73 – 15.19)
In-Plane Translational Distance (<i>mm</i>)	-	6.91(4.06 – 15.21)	9.56(4.95 – 12.77)
Out-of-Plane Translational Distance (<i>mm</i>)	-	2.76(1.86 – 3.17)	1.81(0.70 – 3.16)
Rotational Distance (°)	-	16.36(12.32 – 18.95)	15.88(13.38 – 19.78)
In-Plane Rotational Distance (°)	-	14.80(9.55 – 17.99)	16.75(12.92 – 23.82)
Out-of-Plane Rotational Distance (°)	-	5.24(1.25 – 5.76)	3.80(1.54 – 9.22)
Median Hausdorff Distance (<i>mm</i>)	-	2.93(2.45 – 4.43)	2.78(2.65 – 4.34)
Dice Similarity Coefficient	-	0.22(0.12 – 0.32)	0.23(0.07 – 0.34)

were only available in ten out of twelve cases. Data was assessed for normality using Jarque-Bera test and was found to be non-normally distributed. Data are thus reported as median (inter-quartile range).

The fiducial registration error for the CT to reference tracker registration (see section 2.3) was 7.92(6.52 – 9.73)*mm*, which corresponds to approximate target registration error of 4.19(3.70 – 4.98)*mm* given the fiducial configuration used.²⁰

Overall, the full reconstruction of the septum achieved projected position differences of 2.74(2.06 – 2.81)*mm* and projected orientation differences of 8.95(7.11 – 10.55)° compared to the ground-truth septums, given the optimal hyperparameters from the other septums.

Initial registration (see section 2.2.2) achieved projected position differences of 2.80(2.30 – 3.11)*mm* and projected orientation differences of 9.35(7.35 – 11.54)°. The root mean square error for initial registration was 5.91(5.53 – 7.15)*mm*.

The differences between the reconstructed septums and the ground truth septums are reported in Table 1 for the hyperparameters achieving the best performance on all other septums. Table 1 also includes results using planar fit² and the initial registration.

Full reconstruction of the nasal septum took, on average, 2 minutes and 37 seconds.

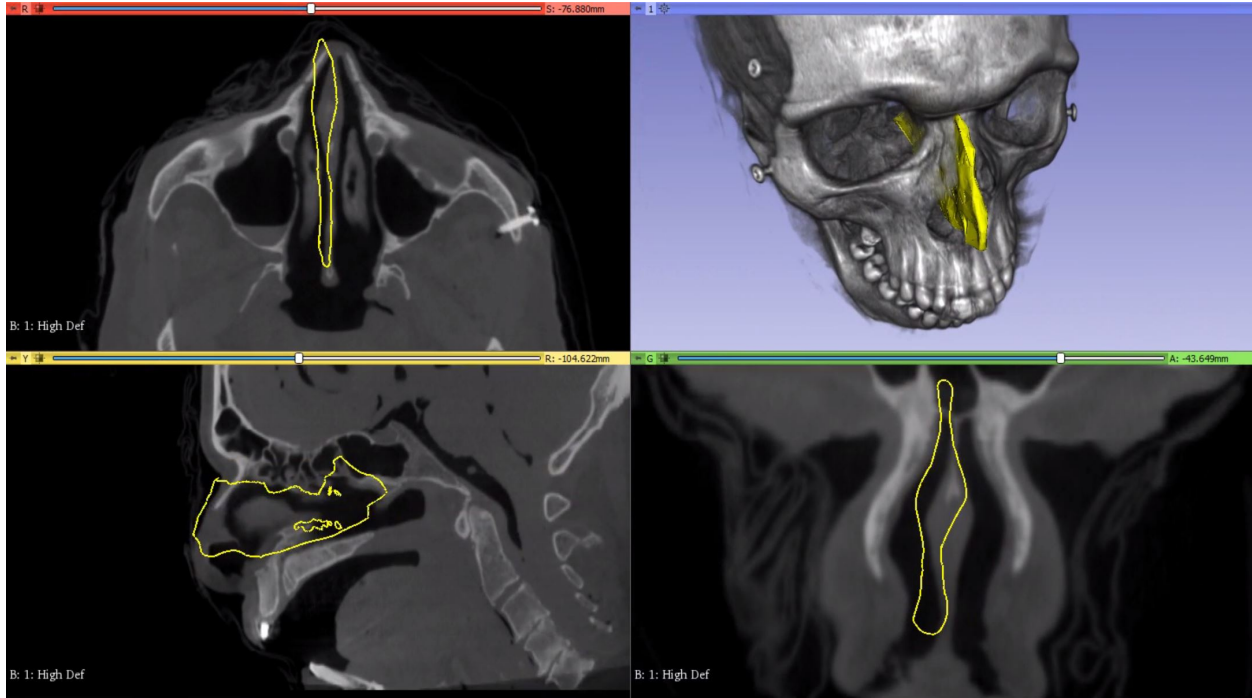


Fig 6 Axial (top-left), sagittal (bottom-left), coronal (bottom-right), and 3D (top-right) views of the reconstructed septum compared to the ground-truth septum in CT. CT image is rendered in 3D view.

1 The effects of the potential confounding variables (i.e. septal deflection and operator skill
 2 level) are reported in Table 2. Of the ten cases with complete data, the median (inter-quartile
 3 range) deflection in the cadaver septums was $1.82(1.44 - 2.42)mm$. Six trials were performed
 4 by experts, and four trials were performed by novices. The only correlation that was statistically
 5 significant was skill and in-plane rotational distance (less error was associated with less skilled
 6 operators); none of the other correlations were statistically significant.

7 **4 Discussion**

8 The proposed method for septum reconstruction succeeded in all cases where there was a complete
 9 dataset available. The reconstruction is performed from data acquired during the surgery, and it
 10 does not require explicit delineation of the septum's surface.

11 The local position error in the proposed reconstructions is $2.74(2.06 - 2.81)mm$ on average,

Table 2 Rank correlation between metrics for septum reconstruction with septal deflection (deflection) and operator skill level (skill). Results are from the full reconstruction method.

Metric	Deflection	Skill
Projected Position Differences (<i>mm</i>)	0.43	0.07
Projected Orientation Differences ($^{\circ}$)	0.10	-0.14
Translational Distance (<i>mm</i>)	0.20	0.28
In-Plane Translational Distance (<i>mm</i>)	-0.36	0.28
Out-of-Plane Translational Distance (<i>mm</i>)	0.43	0.07
Rotational Distance ($^{\circ}$)	-0.21	0.42
In-Plane Rotational Distance ($^{\circ}$)	0.09	0.85
Out-of-Plane Rotational Distance ($^{\circ}$)	-0.13	-0.28
Median Hausdorff Distance (<i>mm</i>)	0.56	0.57
Dice Similarity Coefficient	0.00	-0.28

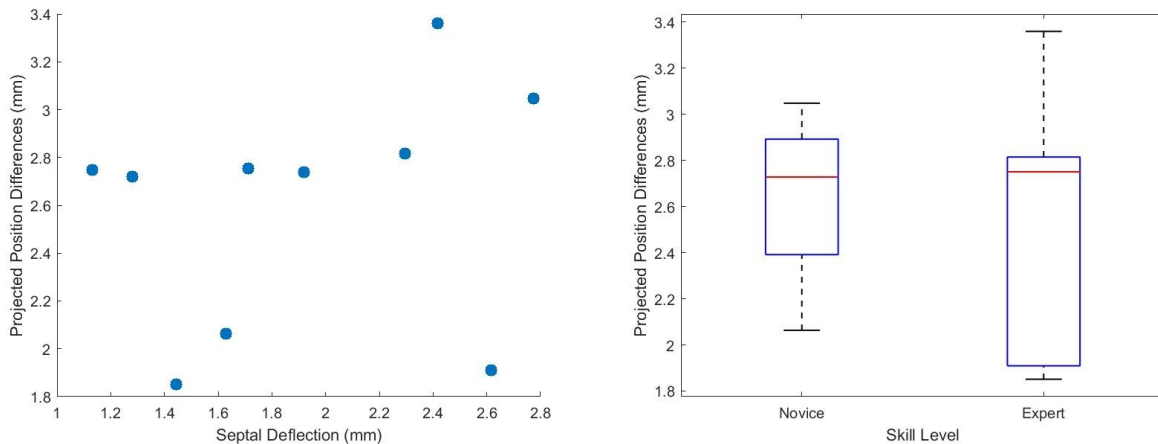


Fig 7 Projected position differences vs. septal deflection (left) and projected position differences vs. operator skill level (right) for the reconstructed septums.

1 given the optimal regularization. This is comparable to accuracy found in surgical navigation sys-
2 tems (and thus suitable for navigation), and it is typical accuracy in co-registration of CT and
3 MRI.²¹ Some of this error can be attributed to the CT to reference tracker registration used to
4 compare the reconstructions to the manually segmented septums, which had an fiducial registra-
5 tion error of $7.92(6.52 - 9.73)mm$. The large fiducial registration error is likely due to magnetic
6 field distortions due to ferromagnetic materials in the operating environment. The target registra-
7 tion error at the centroid of the septum, however, was approximately $4.19(3.70 - 4.98)mm$ given
8 the fiducial configuration.²⁰ Furthermore, we performed a simulation experiment perturbing the
9 fiducial points according to the fiducial localization error²⁰ and observed target registration error
10 $4.41(3.59 - 5.14)mm$, where the magnitude of error out-of-plane was $2.41(2.00 - 2.91)mm$. Fur-
11 ther error could be due to the statistical shape model; it is computed through automated non-linear
12 registration, which may introduce some error in the shape model's modes of variation.

13 The local orientation error is on average $8.95(7.11 - 10.55)^\circ$ in the proposed reconstructions,
14 given the optimal regularization. This exceeds the performance achieved for the optimal planar
15 estimate of the septum (fitted via principal components analysis to the ground-truth septum with
16 thickness equal to the mean thickness of the ground-truth septum), where we observed local ori-
17 entation errors of $9.87(6.35 - 11.21)^\circ$. We note that the local orientation errors are affected by
18 position errors due to the way corresponding points on the reconstructed and ground-truth septums
19 are found. While we filter out instances where the orientation difference in projections is greater
20 than 90 degrees (which indicates corresponding points are on different sides of the septum due
21 to position error), we believe the reported orientation error considerably overestimates the true
22 orientation error.

23 The full reconstruction from elevation data did not significantly improve upon the initial recon-

1 struction and had small effect size, but descriptive statistics indicate some benefit to the proposed
2 reconstruction. We hypothesize the lack of observed improvement is because the cadavers' sep-
3 tums did not have large deflections ($1.82(1.44 - 2.42)mm$), and thus, the added value of the shape
4 model is limited. Indeed, by optimally registering the mean septum to the ground-truth septums, we
5 found local position error of $1.78(1.62 - 2.30)mm$ and local orientation error $7.03(3.38 - 8.27)^\circ$.
6 These values provide loose upper bounds on the added value of the shape modelling for the sep-
7 tums in our dataset. The results are also limited by the small sample size due to expense and limited
8 availability of cadavers.

9 We used the position and orientation difference between corresponding points as the primary
10 measures of accuracy in this work. This is because instrument motion only occurs in one region
11 of the septum and reconstruction will be most valuable in that region. Thus, local measures of
12 accuracy better quantify the utility of the reconstruction. Traditional measures of closed surface
13 comparison and overall measures of pose accuracy are not as useful in this application. In particu-
14 lar, we observe that the Dice Similarity Coefficient is not well-suited for this application due to the
15 thin shape of the septum, which makes it very sensitive to small errors in translation.

16 Initial reconstruction achieves the greatest accuracies for some global reconstruction metrics
17 (i.e overall translational and rotational distance), as this is exactly the quantity that the ICP regis-
18 tration minimizes. The full reconstruction optimizes the local fits, at the expense of the global fit.
19 We observe, however, that global pose error is primarily due to in-plane error. Because the septum
20 is nearly planar, there is a lack of constraints on in-plane translation and rotation. We propose that
21 further annotation could be used to better constraint in-plane translation and rotation, making the
22 problem better posed.

23 The validation study has demonstrated the accuracy of reconstructing the septum in cadavers.

1 The septal deflections observed in our dataset were $1.82(1.44 - 2.42)mm$, while the deflections
2 observed in septums generated randomly from our statistical shape model derived from a general
3 population were $1.44(1.14 - 1.85)mm$. Nasal septoplasty is commonly performed on skull-base
4 surgery or cosmetic surgery patients, whose septal deflections follow the same distribution as the
5 general population. We thus anticipate our results on this cadaver dataset will apply to such sep-
6 toplasty cases. Further issues due to different distributions in septal deflections may be addressed
7 by selecting a larger CT image database which contains data from septoplasty candidates with a
8 greater diversity of pathologies or deflections and building a shape model using from a more repre-
9 sentative set of septums. Tuning of the regularization parameters may also be necessary to capture
10 these greater deviations. Furthermore, we have shown the effect of both deflection and operator
11 skill level on reconstruction accuracy. Our dataset is heterogeneous with respect to operator skill
12 level, like encountered in patient data where surgeries may be performed by attending surgeons or
13 residents of varying skill levels.

14 The proposed methods for septum reconstruction may generalize to anatomical surface recon-
15 struction in other hard tissue applications, with some caveats. One of the challenges of recon-
16 structing the septum from tool tip data is that the thickness of the septum (2mm at its thinnest) is
17 approximately equal to the accuracy of the tracking system. This necessitates the use of orientation
18 information to distinguish tool tip motion on either side of the septum. The proposed method for
19 determining the orientation of trajectory points is specific to reconstruction of the nasal septum.
20 Furthermore, the initial registration phase requires a reliable set of landmarks rigidly connected to
21 the relevant anatomy. This may not be possible to acquire in all interventions.

22 Monitoring instrument trajectories during septoplasty surgery allows reconstruction of the
23 nasal septum at the conclusion of the elevation phase without the need for CT. This enables ob-

1 jective determination of the shape of the septum, which has application in diagnosis of pathology,
2 clinical decision support, and documentation of nasal obstruction for insurance purposes. This also
3 enables real-time virtual endoscopy or other surgical navigation modalities during portions of the
4 surgery after elevation by tracking the instruments relative to the reconstructed septum, which has
5 been shown to have added value in septoplasty.²² Finally, it enables surgical skills assessment in
6 septoplasty by analyzing instrument motion relative to local anatomy and septum shape, which are
7 considerable confounding factors in performance of septoplasty surgery. Indeed, analyzing tool
8 motion relative to anatomy has been shown to have added value in other applications.²³

9 **5 Conclusion**

10 We have proposed a method for reconstructing the nasal septum from instrument motion data dur-
11 ing the elevation phase of septoplasty surgery. The method does not require explicit delineation
12 of the septum. The proposed method succeeded in all cases with complete datasets. We have
13 measured the accuracy of the proposed methods using a dataset of tracked septoplasty surgeries
14 performed on cadavers, and found our reconstructions to be within $2.74(2.06 - 2.81)mm$ and
15 $8.95(7.11 - 10.55)^\circ$ of the true septum, given the optimal regularizations. Our method outper-
16 forms estimates of the septal plane used in prior work.² This work enables computation of the
17 septal anatomy in real-time. This will enable objective computation of septal deviation, surgical
18 navigation, and performance assessment.

19 *Disclosures*

20 The authors have no conflicts of interest to declare.

1 *Acknowledgments*

2 The authors thank Ayushi Sinha for her assistance in computing the statistical shape model of the
3 septum.

4 Matthew S. Holden was supported by the Natural Sciences and Engineering Research Council
5 of Canada (NSERC) Postdoctoral Fellowship (Grant No. PDF-533006-2019). This work was
6 supported by NIH R01-DE025265 and R21-DE022656 (PI: Masaru Ishii).

7 *References*

- 8 1 T. S. De Silva, S. S. Vedula, A. Perdomo-Pantoja, *et al.*, “Spinecloud: image analytics for
9 predictive modeling of spine surgery outcomes,” *Journal of Medical Imaging* **7**(3), 031502
10 (2020).
- 11 2 N. Ahmidi, P. Poddar, J. D. Jones, *et al.*, “Automated objective surgical skill assessment in
12 the operating room from unstructured tool motion in septoplasty,” *International Journal of*
13 *Computer Assisted Radiology and Surgery* **10**, 981–991 (2015).
- 14 3 N. Ahmidi, L. Tao, S. Sefati, *et al.*, “A dataset and benchmarks for segmentation and recog-
15 nition of gestures in robotic surgery,” *IEEE Transactions on Biomedical Engineering* **64**(9),
16 2025–2041 (2017).
- 17 4 S. S. Vedula, M. Ishii, and G. D. Hager, “Objective assessment of surgical technical skill and
18 competency in the operating room,” *Annual review of biomedical engineering* **19**, 301–325
19 (2017).
- 20 5 T. Vaughan, *Generating patient-specific 3D models using a pointing device*. PhD thesis,
21 Queen’s University (2014).

- 1 6 H. Hoppe, T. DeRose, T. Duchamp, *et al.*, *Surface reconstruction from unorganized points*,
2 vol. 26, ACM (1992).
- 3 7 T. F. Cootes, A. Hill, C. J. Taylor, *et al.*, “Use of active shape models for locating structures
4 in medical images,” *Image and vision computing* **12**(6), 355–365 (1994).
- 5 8 S. P. Lim and H. Haron, “Surface reconstruction techniques: a review,” *Artificial Intelligence*
6 *Review* **42**(1), 59–78 (2014).
- 7 9 N. Bhattacharyya, “Ambulatory sinus and nasal surgery in the united states: Demographics
8 and perioperative outcomes,” *The Laryngoscope* **120**(3), 635–638 (2010).
- 9 10 M. Wotman and A. Kacker, “What are the indications for the use of computed tomography
10 before septoplasty?,” *The Laryngoscope* **126**(6), 1268–1270 (2016).
- 11 11 D. Karatas, F. Yuksel, M. Senturk, *et al.*, “The contribution of computed tomography to nasal
12 septoplasty,” *J Craniofac Surg* **24**, 1549–1551 (2013).
- 13 12 E. Gunbey, H. P. Gunbey, S. Uygun, *et al.*, “Is preoperative paranasal sinus computed to-
14 mography necessary for every patient undergoing septoplasty?,” *Int Forum Allergy Rhinol* **5**,
15 839–845 (2015).
- 16 13 N. Fettman, T. Sanford, and R. Sindwani, “Surgical management of the deviated septum:
17 Techniques in septoplasty,” *Otolaryngologic Clinics of North America* **42**(2), 241 – 252
18 (2009). *Surgical Management of Nasal Obstruction*.
- 19 14 A. Sinha, S. Leonard, A. Reiter, *et al.*, “Automatic segmentation and statistical shape model-
20 ing of the paranasal sinuses to estimate natural variations,” in *Medical Imaging 2016: Image*
21 *Processing*, **9784**, 97840D, International Society for Optics and Photonics (2016).

- 1 15 B. B. Avants, N. J. Tustison, G. Song, *et al.*, “A reproducible evaluation of ants similarity
2 metric performance in brain image registration,” *Neuroimage* **54**(3), 2033–2044 (2011).
- 3 16 P. J. Besl and N. D. McKay, “Method for registration of 3-d shapes,” in *Sensor fusion IV:
4 control paradigms and data structures*, **1611**, 586–606, International Society for Optics and
5 Photonics (1992).
- 6 17 S. Billings and R. Taylor, “Iterative most likely oriented point registration,” in *International
7 Conference on Medical Image Computing and Computer-Assisted Intervention*, 178–185,
8 Springer (2014).
- 9 18 T. Heimann and H.-P. Meinzer, “Statistical shape models for 3d medical image segmentation:
10 a review,” *Medical image analysis* **13**(4), 543–563 (2009).
- 11 19 T. Cootes, C. Taylor, D. Cooper, *et al.*, “Active shape models-their training and application,”
12 *Computer Vision and Image Understanding* **61**(1), 38 – 59 (1995).
- 13 20 J. M. Fitzpatrick, J. B. West, and C. R. Maurer, “Predicting error in rigid-body point-based
14 registration,” *IEEE transactions on medical imaging* **17**(5), 694–702 (1998).
- 15 21 D. Guha, N. M. Alotaibi, N. Nguyen, *et al.*, “Augmented reality in neurosurgery: A review
16 of current concepts and emerging applications,” *Canadian Journal of Neurological Sciences
17 / Journal Canadien des Sciences Neurologiques* **44**(3), 235–245 (2017).
- 18 22 C. J. Hong, E. Monteiro, J. Badhiwala, *et al.*, “Open versus endoscopic septoplasty tech-
19 niques: A systematic review and meta-analysis,” *American journal of rhinology & allergy*
20 **30**(6), 436–442 (2016).
- 21 23 M. S. Holden, Z. Keri, T. Ungi, *et al.*, “Overall proficiency assessment in point-of-care ul-

1 trasound interventions: the stopwatch is not enough,” in *Imaging for Patient-Customized*
2 *Simulations and Systems for Point-of-Care Ultrasound*, 146–153, Springer (2017).

3 **List of Figures**

- 4 1 Photograph of a Cottle elevator used for flap elevation during septoplasty surgery.
5 Both tips can be used for elevation.
- 6 2 Photograph of ongoing tracked septoplasty surgery (left) and diagram of data col-
7 lection setup (right).
- 8 3 Block diagram illustration of the proposed method for reconstructing the nasal
9 septum.
- 10 4 Sagittal (left) and coronal (right) views of fiducial points selected on nose circle
11 (red) and nose line (green) on the dorsum in the template CT image.
- 12 5 Initial (blue) and full (green) reconstructions of the septum from Cottle tip trajec-
13 tory, with the ground-truth septum (red) for the axial (left), sagittal (centre), and
14 coronal (right) views. Points along the trajectory with their estimated orientation
15 are illustrated (cyan and black). Nose circle (yellow) and nose line (magenta) il-
16 lustrated.
- 17 6 Axial (top-left), sagittal (bottom-left), coronal (bottom-right), and 3D (top-right)
18 views of the reconstructed septum compared to the ground-truth septum in CT. CT
19 image is rendered in 3D view.
- 20 7 Projected position differences vs. septal deflection (left) and projected position
21 differences vs. operator skill level (right) for the reconstructed septums.

1 List of Tables

2 1 Accuracy metrics for septum reconstruction. Results from the planat fit (planar),²
3 initial registration (initial), and for the full reconstruction (full). Values are reported
4 as median (inter-quartile range). The best performing method for each metric is
5 indicated in bold.

6 2 Rank correlation between metrics for septum reconstruction with septal deflection
7 (deflection) and operator skill level (skill). Results are from the full reconstruction
8 method.